

Detecting Phase-Resolved Magnetization Dynamics by Magneto-Optic Effects at 1550 nm Wavelength

Yuzan Xiong^{1,2}, Yi Li³, Rao Bidhanapally¹, Joseph Sklenar⁴, Mouhamad Hammami¹, Sawyer Hall¹, Xufeng Zhang⁵, Peng Li⁶, John E. Pearson³, Thomas Sebastian⁷, Gopalan Srinivasan¹, Axel Hoffmann^{3,8}, *Fellow, IEEE*, Hongwei Qu², Valentine Novosad³, and Wei Zhang^{1,3}

¹Department of Physics, Oakland University, Rochester, MI 48309 USA

²Department of Electronic and Computer Engineering, Oakland University, Rochester, MI 48309 USA

³Materials Science Division, Argonne National Laboratory, Argonne, IL 60439 USA

⁴Department of Physics and Astronomy, Wayne State University, Detroit, MI 48201 USA

⁵Center for Nanoscale Materials, Argonne National Laboratory, Argonne, IL 60439 USA

⁶Department of Electrical and Computer Engineering, Auburn University, Auburn, AL 36849 USA

⁷THATec Innovation GmbH, 68165 Mannheim, Germany

⁸Department of Materials Science and Engineering, University of Illinois at Urbana–Champaign, Urbana, IL 61801 USA

We demonstrate the detection of phase-resolved magnetization dynamics with combinatorial magneto-optic Kerr and Faraday effects. The method uses a continuous-wave laser that is amplitude-modulated at the spin dynamic frequencies and thus allows for coherent tracking of the spin dynamics, akin a “lock-in”-type measurement. In particular, our method, using a single 1550 nm wavelength, probes simultaneously the ferromagnetic (FM) resonance of $\text{Y}_3\text{Fe}_5\text{O}_{12}$ (YIG) and Permalloy ($\text{Py} = \text{Ni}_{80}\text{Fe}_{20}$) in a YIG-Py heterostructure. The fiber-based magneto-optic components also have the advantage of being made into a compact, tabletop or even portable system with yet robust measurement performances. We believe that our method will be found useful in studying hybrid quantum magnonic systems and/or investigating phase-resolved spin dynamics in nanomagnet structures involving both FM insulators and metals.

Index Terms—Epitaxial films, ferromagnetic resonance (FMR), IEEE, IEEE TRANSACTIONS ON MAGNETICS, IEEEtran, optical detection.

I. INTRODUCTION

THE needs for sensitively and reliably probing the magnetization dynamics have been increasing in various contexts [1] and especially in novel spintronic and magnonic research [2]–[6], where the spin and magnon dynamics are driven by the state-of-the-art approaches using spin torques [7], acoustic phonons [8], spin-thermo effects [9], [10], and microwave photons [11], [12]. Recent breakthroughs in quantum magnonics [13] also highlight the needs for detecting spatial- and phase-resolved magnetization dynamics adaptable to micro- and nano-scale magnonic devices with synergistic photonic and spin-electronic components on-chip [14], [15].

To date, optical detection of magnetization dynamics is performed predominantly by pump-probe and related techniques, in which a series of probing laser pulses is delayed at different temporal positions to track the ultrafast dynamics, following an initial pump pulse [16]–[19]. The experimental setup usually involves expensive lasers and complex optical layouts, including, for example, a well-aligned opto-mechanical delay line. Another technique is Brillouin light scattering (BLS) [20], which makes use of the inelastic

scattering of laser light photons with magnons and/or phonons. This method offers good spatially and wave-vector-resolved mapping of spin-wave intensity but is time-consuming and noise-sensitive to filter out the wavelength offset, especially for lower frequencies. Furthermore, the different optical and dielectric properties of samples (e.g., metals, semiconductors, or insulators) also often times require to use different probe wavelengths in the visible (VIS) range, which can further complicate the measurement [21].

In this work, we demonstrate the detection of phase-resolved magnetization dynamics, which combines different magneto-optic effects. This method uses a 1550 nm laser in the near-infrared (NIR) wavelength band, which allows facile modulation at the gigahertz frequencies with both amplitude control and phase control and also phase-locking to a microwave source for the excitations of magnetization dynamics. Such a continuous-wave (CW) modulation capability makes this particular wavelength-band advantageous for studying magnetization dynamics in complex magnetic systems, such as quantum magnonic hybrids, patterned nanomagnets, and spin ice. Compared to VIS-light wavelengths for magneto-optics [22], [23], our method allows for the coherent tracking of gigahertz spin dynamics in a CW fashion, very much resembling a “lock-in” type of measurement that is commonly performed in many low-noise electric and spin transport measurements. In addition, the fiber-based optics allow for a facile integration with simultaneous electrical, thermal, and magnetic measurements. From a technological

Manuscript received April 29, 2020; revised July 13, 2020; accepted July 27, 2020. Date of publication July 30, 2020; date of current version January 20, 2021. Corresponding authors: V. Novosad and W. Zhang (e-mail: novosad@anl.gov; weizhang@oakland.edu).

Color versions of one or more of the figures in this article are available online at <https://ieeexplore.ieee.org>.

Digital Object Identifier 10.1109/TMAG.2020.3013063

0018-9464 © 2020 IEEE. Personal use is permitted, but republication/redistribution requires IEEE permission.

See <https://www.ieee.org/publications/rights/index.html> for more information.

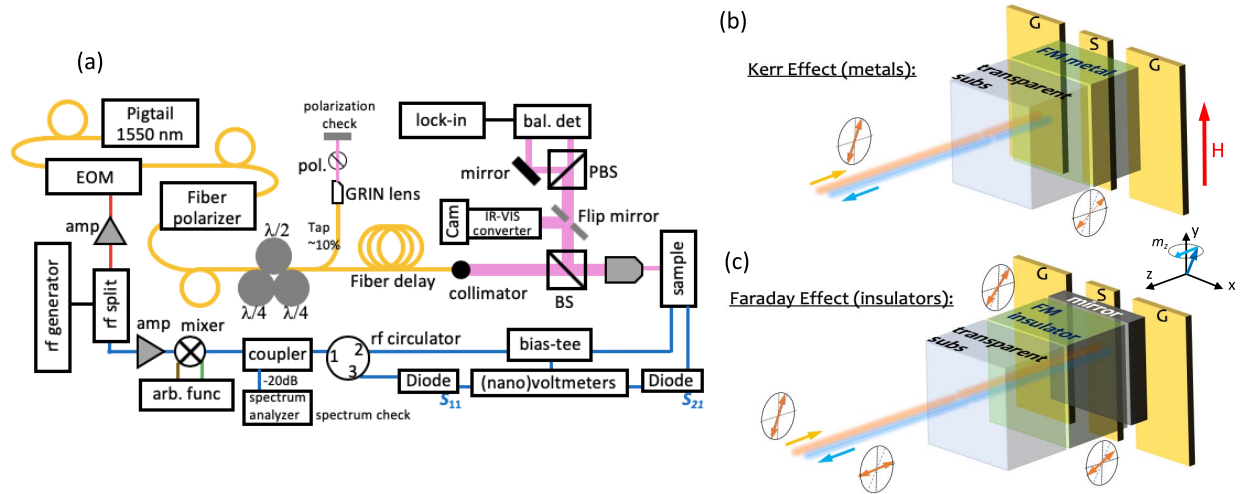


Fig. 1. (a) Schematics of the measurement setup. After the rf splitter, the optical path (upper part) contains amplifier, 1550 nm infrared laser module, EOM, fiber polarizer, fiber polarization controller, beam splitter (BS), and focusing lens; the electrical path (lower part) contains amplifier, mixer, coupler, spectrum analyzer, diodes, circulator, bias-tee, and nanovoltmeter. PBS = polarizing BS, Cam = camera, bal.det = balanced detector, and arb. func = arbitrary waveform generator. (b) and (c) Schematic of the detecting mechanism for the dynamic Kerr and Faraday effects, respectively. For Kerr effect detection, the modulated and linearly polarized 1550 nm light first hits the sample surface at a certain polarization angle, then, the dynamic Kerr effect due to the FMR excitation causes a rotation of the polarization, which is subsequently analyzed. For Faraday effect detection, the incoming light first enters the sample at a polarization angle, then, the dynamic Faraday effect due to the FMR excitation causes the polarization to rotate, next, the light hits the mirror and the reflected light, upon the returning path, picks up again the Faraday effect, and causes the polarization to further rotate along the same direction, before the subsequent light analysis. The applied dc magnetic field is parallel to the ground-signal-ground (G-S-G) lines of the CPW.

point of view, fiber-based magneto-optic systems are also less susceptible to typical mechanical vibrations compared with real-space optical systems [23]–[28]. Therefore, they have the advantage of being made into compact, tabletop or even portable systems with yet robust measurement performances.

Earlier, it has been demonstrated that the CW 1550 nm magneto-optics can be used to sensitively probe phase-resolved magnetization dynamics via the magneto-optic Kerr effect [29] of ferromagnetic (FM) metals, in both inductive [30], [31] and spin-torque FM resonance (FMR) [32] configurations. However, it remains a question whether such a technique can be extended to probing similar gigahertz spin dynamics for FM insulators, which are typically non-reflective at the NIR wavelengths. Here, we show that the 1550 nm system can be indeed used for probing phase-resolved FMR for FM insulators, via the magneto-optic Faraday effect, and we demonstrate such capability by using $\text{Y}_3\text{Fe}_5\text{O}_{12}$ (YIG) thin films, a widely used FM insulator in the current spintronics research [33].

II. EXPERIMENTAL SETUP

Fig. 1(a) shows a schematic of the experimental setup. The magnetization dynamics are detected optically, via either the magneto-optic Kerr (for FM metals) or Faraday (for FM insulators) effects. The laser is normal incident on the thin-film samples, and thus, both effects are sensitive to the out-of-plane component of the precessing magnetization, m_z . A heterodyne method is adopted to enable precessional phase tracking [30]–[32]. A single microwave source is used to simultaneously modulate the laser (optical path) and drive the FMR of the sample (electrical path) with a coplanar waveguide (CPW). The laser light is modulated at the microwave source frequency using an electro-optic intensity modulator (EOM).

The modulated laser light can be polarized by either a fiber polarizer (e.g., a 3 paddle $\lambda/4, \lambda/2, \lambda/4$ controller) or a free-space thin-film polarizer, before being collimated and focused onto the sample surface. We also use an optical tap ($\sim 10\%$), a graded-index (GRIN) lens, and another free-space polarizer to monitor the polarization state and the light intensity throughout the whole measurements, which is especially useful when working with the all-fiber-based polarizing systems. The focused light spot is around $\sim 40 \mu\text{m}$ in the present work. The out-of-plane magnetization is dynamically probed via the Kerr or Faraday responses of the samples. The changing polarization states are subsequently analyzed with a polarization beam splitter and a balancing detector and then a lock-in amplifier. Before performing the optical measurement, sample imaging and fine alignment can be made via the flip mirror, which detours the light path to an IR-VIS converter and a CMOS camera. It is also noted that by adopting fiber-based laser components and optical cage systems, the whole setup can be made into a compact form taking a total space less than 14 in \times 14 in.

For a heterodyne detection, the microwave signal along the electrical path is in-phase (I) and quadrature (Q)-mixed with a low-frequency (100 kHz) signal provided by an arbitrary function generator. The voltage amplitude, offset, and phase for the respective “I” and “Q” channels are optimized to ensure that the power of the upper sideband of the microwave signal (which is subsequently used for FMR excitation) far exceeds those of the central and lower sideband (>20 dB). We use a directional coupler (-20 dB) and a real-time spectrum analyzer to monitor the central and sidebands throughout the whole measurement. The main microwave line then goes through a microwave circulator (and/or a bias tee) before reaching the sample. Microwave diode can

be used to simultaneously measure either the reflection or the transmission (similar to vector-network-analyzers (VNAs) S_{11} or S_{21}) of the inductive FMR, through the CPW and the (nano-)voltmeters.

The automated control of all devices in our experimental setup and the data acquisition are achieved with the software platform thaTEC:OS [34] from a central user interface. The module concept behind thaTEC:OS allows for a fast integration of new devices during the development phase as well as an easy adjustment of the measurement protocol in the daily lab work. Furthermore, it opens the perspective to future extensions of instruments with minimal programming efforts. An obvious extension that highlights the potential of the presented approach is the incorporation of a (nano-)positioning system and a better viewing system, including an objective lens to allow for the space-resolved investigation of spin dynamics at the mesoscale.

III. SAMPLES AND DETECTING MECHANISM

The detection of the magneto-optic Kerr effect for FM metals has been demonstrated in our earlier work based on the spin-torque FMR configuration using a similar setup [32]. Here, we focus on the inductive FMR configuration and demonstrate one measurement for an MgO/Fe(10 nm)/Pt(3 nm cap) thin-film bilayer, although the mechanism is actually the same. It is noted that the MgO substrate has to be double-side-polished to allow the laser light to access from the backside, as shown in Fig. 1(b).

On the other hand, to demonstrate the Faraday detection capability of the system, we use commercial YIG films (from MTI Corporation) with thickness $t_{\text{YIG}} = 3 \mu\text{m}$, single-sided grown on double-side-polished Gd₃Ga₅O₁₂ (GGG) substrates via liquid phase epitaxy (LPE). Next, we grew a nonmagnetic metal layer of Pt, Cu, and Ag, with thicknesses, $t_{\text{Pt(Cu,Ag)}} = 30 \text{ nm}$, on top of the YIG to make a reflective mirror for the optical path.

We also prepared a YIG/SiO₂(3 nm)/Permalloy (Py, 30 nm) sample, for studying the combinatorial Kerr and Faraday detection. We use the 3 nm SiO₂ interlayer for the Py-sample to purposely avoid the possible magnon–magnon coupling due to interface exchange interaction [36]–[40] between YIG and Py.

All the metal films are deposited using the magnetron sputtering at low deposition rates, to minimize the surface roughness and thus ensure a good light reflection. In addition, we also use *in situ* Ar gas rf-bias cleaning for 3 min, to clean the YIG surface right before depositing the metal layers.

Fig. 1(c) shows the detecting mechanism for the YIG Faraday effect. The modulated and linearly polarized 1550 nm light passes through the transparent GGG substrates. Next, as the light travels through the YIG bulk, the dynamic Faraday rotation due to the YIG FMR is picked up. Then, the metal layer serves as a mirror and reflects the laser light. Upon reflection, the dynamic Faraday effect from the YIG is picked up again, making the effective YIG thickness 6 μm , i.e., twice the film thickness. It should be noted that the Faraday rotations for the incoming and returning light add up as opposed to cancel, due to the reflection at the metal layers, whose

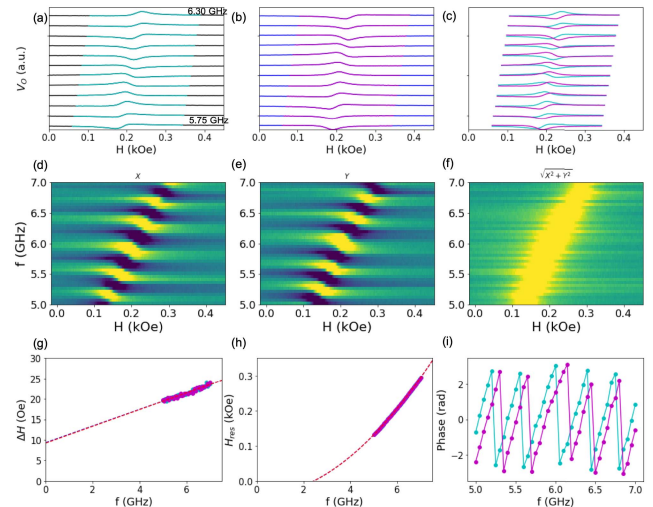


Fig. 2. Selective optically detected FMR traces (5.75–6.3 GHz) of the Fe/Pt bilayer (a) with the in-phase, X , (b) quadrature, Y components, and (c) extracted field region for FMR analysis. The intensity map of the full scan (5.0–7.0 GHz) of (d) X , (e) Y , and (f) total amplitude, $(X^2 + Y^2)^{1/2}$, as a function of the magnetic field and frequency. Summary of (g) linewidth, (h) resonance field, H_{res} , and the corresponding Kittel fits, and (i) phase evolution with the frequency is also presented.

mechanism is akin to a commercial “Faraday rotator” often encountered in fiber optics.

The YIG samples are chip-flipped on a CPW for microwave excitation and optical detection. An in-plane magnetic field, H , along the y -direction saturates the YIG magnetization. We scan the frequency and the magnetic field and then measure the optical responses using the in-phase X and quadrature Y channels of a lock-in amplifier as well as the microwave transmissions using the microwave diodes.

IV. RESULTS AND DISCUSSION

A. Respective Kerr and Faraday Detection

First, we demonstrate separately the detection of the Kerr and Faraday effect in a metal (Fe) and insulator (YIG), respectively. Fig. 2 shows the representative traces, intensity map, and analysis of the optical signals detected for the Fe/Pt bilayer via the magneto-optic Kerr effect, as a function of magnetic field H and frequency f . On the other hand, Fig. 3 shows the corresponding traces and the intensity map of the optical signals detected for YIG/Ag, YIG/Cu, and YIG/Pt bilayers via the magneto-optic Faraday effect. These results demonstrate the representative features of our detection capability. The optical signals with the phase information are obtained by the lock-in amplifier’s in-phase X and quadrature Y , following:

$$\begin{aligned} X &\propto m_z P_0 \cos(\phi_L - \phi_m) \\ Y &\propto -m_z P_0 \sin(\phi_L - \phi_m) \end{aligned} \quad (1)$$

where m_z is the z -component of the dynamic magnetization, P_0 is the laser light intensity, ϕ_L is the phase accumulated due to the optical path length, and ϕ_m is the magnetization phase, which includes contributions due to ϕ_{MW} (the microwave path), ϕ_h (possible phase delay between waveguide current and effective driving field, h_{rf}), and ϕ_{χ} (the phase of the magnetic

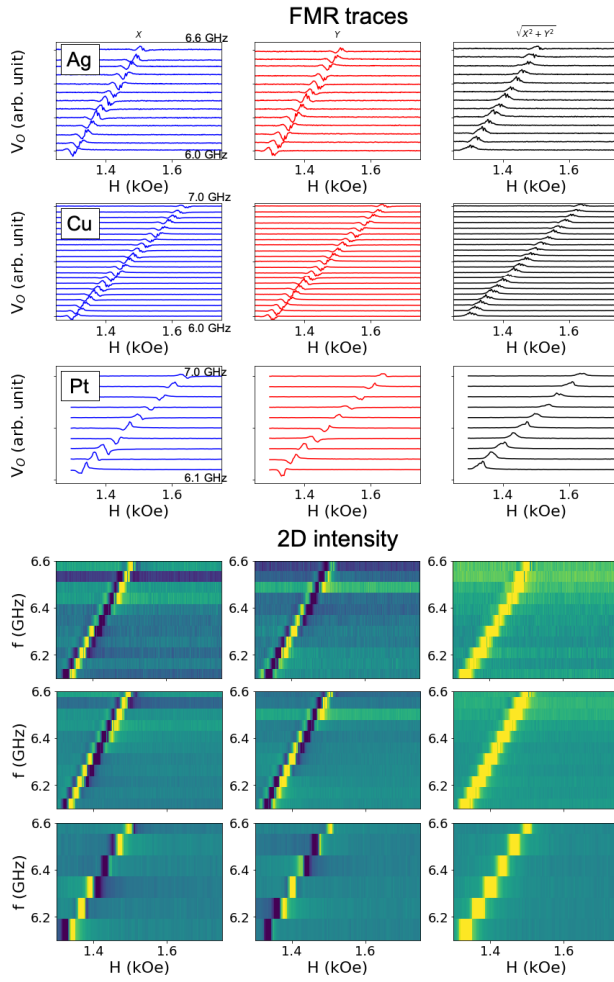


Fig. 3. Top: optically detected FMR traces with the in-phase, X , quadrature, Y components, and the total amplitude, $(X^2 + Y^2)^{1/2}$ as a function of the magnetic field and frequency, for different nonmagnetic mirror materials, Ag, Cu, and Pt. Bottom: intensity maps (shown from 6.1 to 6.6 GHz for all samples) indicate clear and similar phase evolution in the X and Y components for all samples.

response to the field) [30]. The phases ϕ_L and ϕ_{MW} are dependent on the optical and electrical paths, respectively, and the path difference can be tuned by the fiber and microwave-cable lengths or using a microwave phase shifter [32]. The on-resonance phase variation is clearly seen for Fe (Fig. 2) and YIG (Fig. 3), respectively. In addition, an observable bright-dark oscillation of the off-resonance background signal appears for the metallic Fe/Pt, in Fig. 2(d)–(e), which has been reported in the electrical rectification measurements of similar structures [35]. This also reflects the light path associated with phase variation at different frequencies. We noted that the fiber-optic system makes it particularly convenient to engineer the path difference by simply adding optical fibers at desirable lengths. The intensity maps show consistent phase evolution for all samples. The total amplitude is calculated by $(X^2 + Y^2)^{1/2}$, which resembles the conventional microwave diode or the VNA measurements. In our measurements, we fixed the experimental setup for all the samples, and thus, the optical signals should have a negligible effect from ϕ_L , ϕ_{MW} , and ϕ_h . Detailed FMR analysis will be discussed later.

B. Combinatorial Kerr and Faraday Detection

Next, we move to the main result of the work, which is the simultaneous detection of the YIG and Py FMRs via the combination of dynamic Faraday and Kerr effects. The detecting mechanism is a combination of Fig. 1(b) and (c). The modulated and linearly polarized 1550 nm light first passes through the transparent GGG substrates and then travels through the YIG bulk, in which the dynamic Faraday rotation due to the YIG FMR is picked up. Similarly, the dynamic Kerr rotation caused by the Py FMR is then picked up when the light reaches the Py layer. The Py layer also serves as a mirror and reflects the laser light. Upon reflection, the dynamic Faraday effect from the YIG is picked up again before entering the subsequent light analysis.

The experimental results are summarized in Fig. 4. The YIG FMR at higher magnetic fields is the signal from the Faraday effect due to the uniform YIG magnetization precession, detected as

$$X_{\text{YIG}} \propto m_z(\text{YIG}) P_0 \cos [\phi_L - \phi_{\text{MW}} - \phi_h - \phi_{\chi(\text{YIG})}]$$

$$Y_{\text{YIG}} \propto -m_z(\text{YIG}) P_0 \sin [\phi_L - \phi_{\text{MW}} - \phi_h - \phi_{\chi(\text{YIG})}]. \quad (2)$$

The Py FMR at lower magnetic fields, on the other hand, is due to the Kerr effect, detected as

$$X_{\text{Py}} \propto m_z(\text{Py}) P_0 \cos [\phi_L - \phi_{\text{MW}} - \phi_h - \phi_{\chi(\text{Py})}]$$

$$Y_{\text{Py}} \propto -m_z(\text{Py}) P_0 \sin [\phi_L - \phi_{\text{MW}} - \phi_h - \phi_{\chi(\text{Py})}]. \quad (3)$$

Fig. 4(a) shows the intensity map of the optically detected signals X , Y , and the total amplitude $((X^2 + Y^2)^{1/2})$ for the YIG-Py sample as a function of magnetic field H and frequency f from 5.0 to 6.0 GHz at a step size of 0.05 GHz. The FMR modes corresponding to the spatially uniform magnetization precession are described by the Kittel formula: $\omega^2/\gamma^2 = \mu_0^2 H_{\text{res}}(H_{\text{res}} + M_s)$, where ω is the mode frequency, $\gamma/2\pi = (g_{\text{eff}}/2) \times 28 \text{ GHz/T}$ is the gyromagnetic ratio, H_{res} is the resonance field, and M_s is the magnetization.

From Fig. 2, we extract the FMR properties of Fe, yielding $\mu_0 M_s^{\text{Fe}} \sim 1.65 \text{ T}$, and a damping value of ~ 0.003 (note that this value may include the spin pumping effect due to the additional Pt cap). The linewidths, ΔH_{Fe} , resonance fields ($H_{\text{res}}^{\text{Fe}}$), and the phase evolution, extracted from the X and Y channels, are subsequently plotted in Fig. 2(g)–(i).

From the YIG/Py data, we extract the FMR of YIG, in Fig. 4(b), and Py, in Fig. 4(c), respectively, and plot and fit the individual trace segments using the Kittel formula. In our measured frequency window, the two resonances are well separated [see Fig. 4(d)]. The fittings yields the M_s values for YIG and Py, i.e., $\mu_0 M_s^{\text{YIG}} = 0.199 \text{ T}$ and $\mu_0 M_s^{\text{Py}} = 0.907 \text{ T}$, respectively. The linewidths, $\Delta H_{\text{Py(YIG)}}$, resonance fields ($H_{\text{res}}^{\text{Py(YIG)}}$), and the phase evolution are subsequently plotted in Fig. 4(e)–(g).

A clear phase evolution can be observed in the optical signals [see Fig. 4(a)], and in Fig. 4(g), we plot the phase evolution with the frequency for both YIG and Py. The periods of the phase accumulation are the same for both YIG and Py lines, due to the fixed path difference of the measurement geometry. Linear fits with the phase evolution, following $\Delta\phi_{\text{opt/ele}} = (2\pi f/c) \Delta L_{\text{opt/ele}}$, yield an optical/electrical path

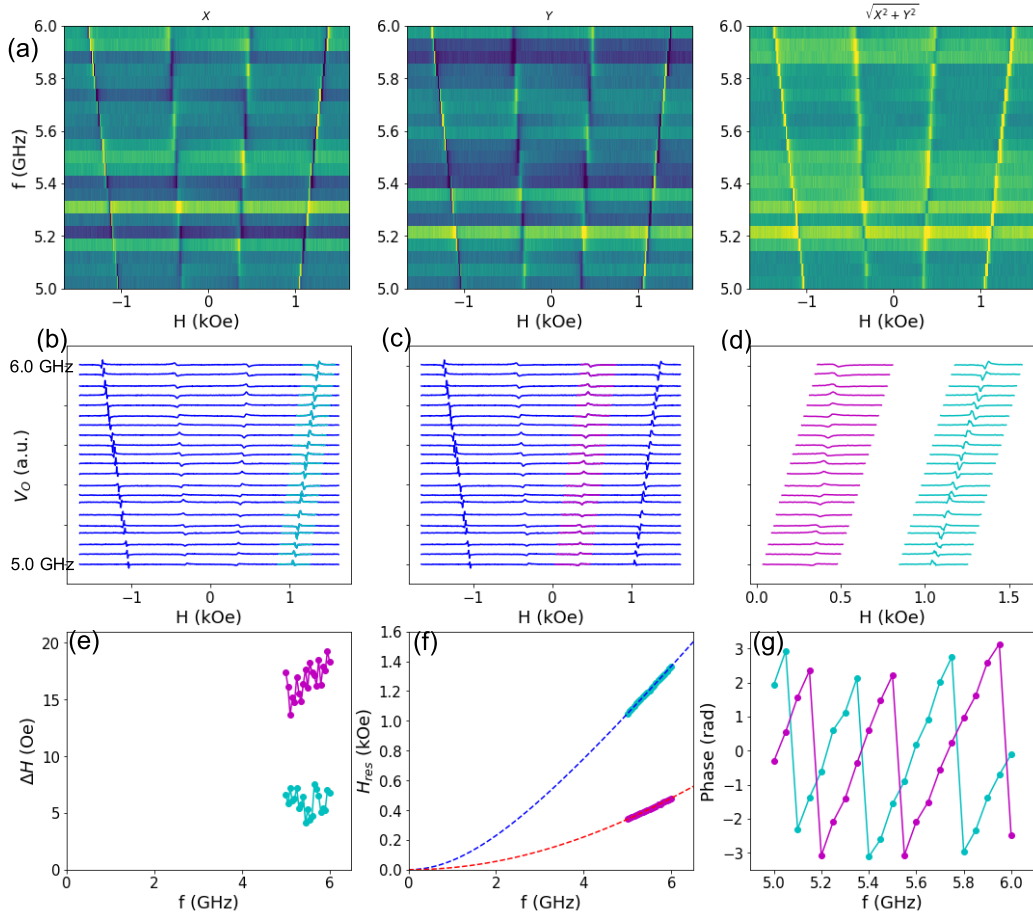


Fig. 4. (a) Intensity map showing the optically detected in-phase, X , quadrature, Y , and the total amplitude ($(X^2 + Y^2)^{1/2}$) as a function of the magnetic field and frequency, for the YIG/SiO₂/Py sample. The optical- X signal traces are shown, with the YIG and Py FMR regimes highlighted, in (b) and (c), respectively. (d) Extracted FMR traces for YIG and Py, which are subsequently fitted with the Kittel formula. (e) Summary of the linewidth, (f) resonance field, H_{res} , and the corresponding Kittel fits, and (g) phase evolution with the frequency is presented.

difference, $\Delta L_{\text{opt/ele}} \sim 75.2$ cm. In addition, a large phase offset of $\sim 2.42 \pm 0.13$ rad exists between the two layers. Note that the two FMR measurements share the same light path, this phase offset, therefore, solely implies the phase difference between the Faraday and Kerr detection. One possible explanation is that there exists a nonzero phase shift of the microwave field from the Py layer to the YIG layer (along the z -direction) due to our planar excitation geometry similar to the previous report [31]. Another possibility is that the reflection of the laser light by a metal (Py in our case) may induce a nonmagnetic shift of the light polarization, which can also impact the phase offset herein.

Finally, we note that the conventional FMR detection via the microwave transmission can be simultaneously performed with this setup from the electrical path, serving as a reference for the optical detection component. In addition, the technical aspects, including the optical/electrical phase modulation using either an optical delay, a phase shifter, or microwave cables, though not shown here, remain valid as demonstrated in our previous works [31], [32]. The diode-detected FMR for the YIG/SiO₂/Py sample is shown in Fig. 5, which, overall, should resemble the total amplitude, $(X^2 + Y^2)^{1/2}$, of the optical signal. However, we found that in the diode signal, the Py

FMR is greatly attenuated compared to the YIG FMR. This is very likely due to the much thicker YIG films (3 μ m) than the Py (30 nm). However, such a difference in their signal magnitudes is not as significant as in the optical detection, as shown in Fig. 4. The YIG Faraday signal is only about one order of magnitude larger than the Py Kerr signal. This fact suggests a potential advantage in resolving the magnetization dynamics of heterostructures involving thick-YIG films and thin-metal layers, such as Py, Co, and Fe, which are often encountered in the study of hybrid magnon-magnon coupled systems [36]–[40].

In summary, we demonstrate the detection of phase-resolved magnetization dynamics with combinatorial magneto-optic Kerr and Faraday effects, which, in particular, can probe simultaneously the FMR of YIG and Py in a YIG/Py bilayer. The method uses a CW laser that is amplitude-modulated at the spin dynamic frequencies and thus allows for coherent tracking of the spin dynamics. Therefore, the method shares the same advantages with conventional lock-in based, field-sweep FMR measurements with high magnetic field resolution and broad dynamic range. In addition, the use of a CW laser and fiber optics greatly simplifies the optical setup, allowing the system to be much less susceptible to external mechanical

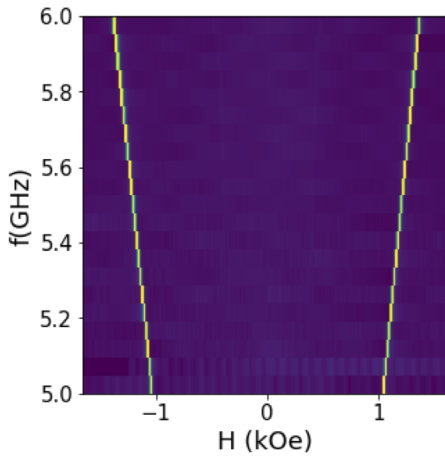


Fig. 5. Microwave transmission signal of the YIG/SiO₂/Py sample acquired simultaneously with the optical detection using a microwave diode.

vibrations and noises, therefore eliminating the possible optical artifacts associated with time-delay-based techniques, with also the potential advantages of being made into a compact, tabletop or even portable system with yet robust measurement performances. Other technical benchmarks, such as characterization speed, spatial/temporal resolutions, and the possible integration with low-temperature environments shall be similar to other optical measurement techniques. We believe that this method will be found useful in studying hybrid quantum magnonic systems and/or investigating phase-resolved spin dynamics in nanomagnet structures [41], [42] and multilayer systems [43], [44] involving both FM insulators and metals.

ACKNOWLEDGMENT

This work was supported in part by the Air Force Office of Scientific Research (AFOSR) under Grant FA9550-19-1-0254, in part by the National Science Foundation under Grant ECCS-1933301 and Grant ECCS-1941426, and in part by the U.S. Department of Energy (DOE), Office of Science, Materials Sciences and Engineering Division. The work of Mouhamad Hammami was supported by the Michigan Space Grant Consortium Student Fellowship.

REFERENCES

- [1] V. V. Kruglyak, S. O. Demokritov, and D. Grundler, "Magnonics," *J. Phys. D, Appl. Phys.*, vol. 43, no. 26, 2010, Art. no. 264001.
- [2] W. Zhang *et al.*, "Spin pumping and inverse spin Hall effects—Insights for future spin-orbitronics (invited)," *J. Appl. Phys.*, vol. 117, no. 17, 2015, Art. no. 172610.
- [3] A. Hoffmann and S. D. Bader, "Opportunities at the frontiers of spintronics," *Phys. Rev. A, Gen. Phys.*, vol. 4, no. 4, Oct. 2015, Art. no. 047001.
- [4] A. V. Chumak, V. I. Vasyuchka, A. A. Serga, and B. Hillebrands, "Magnon spintronics," *Nature Phys.*, vol. 11, no. 6, pp. 453–461, Jun. 2015.
- [5] D. Sander *et al.*, "The 2017 magnetism roadmap," *J. Phys. D, Appl. Phys.*, vol. 50, no. 36, 2017, Art. no. 363001.
- [6] Y. Li, W. Zhang, V. Tyberkevych, W.-K. Kwok, A. Hoffmann, and V. Novosad, "Hybrid magnonics: Physics, circuits and applications for coherent information processing," 2020, *arXiv:2006.16158*. [Online]. Available: <http://arxiv.org/abs/2006.16158>
- [7] A. Manchon *et al.*, "Current-induced spin-orbit torques in ferromagnetic and antiferromagnetic systems," *Rev. Mod. Phys.*, vol. 91, no. 3, Sep. 2019, Art. no. 035004.
- [8] M. Weiler *et al.*, "Elastically driven ferromagnetic resonance in nickel thin films," *Phys. Rev. Lett.*, vol. 106, no. 11, Mar. 2011, Art. no. 117601.
- [9] S. R. Boona, R. C. Myers, and J. P. Heremans, "Spin caloritronics," *Energy Environ. Sci.*, vol. 7, no. 3, p. 885, 2014.
- [10] A. Sola *et al.*, "Spincaloritronic measurements: A round robin comparison of the longitudinal spin Seebeck effect," *IEEE Trans. Instrum. Meas.*, vol. 68, no. 6, pp. 1765–1773, Jun. 2019.
- [11] X. Zhang, C.-L. Zou, L. Jiang, and H. X. Tang, "Strongly coupled magnons and cavity microwave photons," *Phys. Rev. Lett.*, vol. 113, no. 15, Oct. 2014, Art. no. 156401.
- [12] L. Bai, M. Harder, Y. P. Chen, X. Fan, J. Q. Xiao, and C.-M. Hu, "Spin pumping in electrodynamically coupled magnon-photon systems," *Phys. Rev. Lett.*, vol. 114, no. 22, Jun. 2015, Art. no. 227201.
- [13] D. Lachance-Quirion, Y. Tabuchi, A. Gloppe, K. Usami, and Y. Nakamura, "Hybrid quantum systems based on magnonics," *Appl. Phys. Express*, vol. 12, no. 7, Jul. 2019, Art. no. 070101.
- [14] Y. Li *et al.*, "Strong coupling between magnons and microwave photons in on-chip ferromagnet-superconductor thin-film devices," *Phys. Rev. Lett.*, vol. 123, no. 10, Sep. 2019, Art. no. 107701.
- [15] J. T. Hou and L. Liu, "Strong coupling between microwave photons and nanomagnet magnons," *Phys. Rev. Lett.*, vol. 123, Sep. 2019, Art. no. 107702.
- [16] A. Kirilyuk, A. V. Kimel, and T. Rasing, "Ultrafast optical manipulation of magnetic order," *Rev. Mod. Phys.*, vol. 82, no. 3, pp. 2731–2784, Sep. 2010.
- [17] F. B. Moshenok *et al.*, "Broadband conversion of microwaves into propagating spin waves in patterned magnetic structures," *Appl. Phys. Lett.*, vol. 111, no. 4, Jul. 2017, Art. no. 042404.
- [18] M. Deb *et al.*, "Damping of standing spin waves in bismuth-substituted yttrium iron garnet as seen via the time-resolved magneto-optical kerr effect," *Phys. Rev. A, Gen. Phys.*, vol. 12, no. 4, Oct. 2019, Art. no. 044006.
- [19] C. O. Avci *et al.*, "Interface-driven chiral magnetism and current-driven domain walls in insulating magnetic garnets," *Nature Nanotechnol.*, vol. 14, no. 6, pp. 561–566, Jun. 2019.
- [20] T. Sebastian, K. Schultheiss, B. Obry, B. Hillebrands, and H. Schultheiss, "Micro-focused Brillouin light scattering: Imaging spin waves at the nanoscale," *Frontiers Phys.*, vol. 3, p. 35, Jun. 2015.
- [21] A. Kehlberger *et al.*, "Enhanced magneto-optic kerr effect and magnetic properties of Ce₂Fe₅O₁₂ epitaxial thin films," *Phys. Rev. A, Gen. Phys.*, vol. 4, Jul. 2015, Art. no. 014008.
- [22] M. C. Onbasli *et al.*, "Optical and magneto-optical behavior of cerium yttrium iron garnet thin films at wavelengths of 200–1770 nm," *Sci. Rep.*, vol. 6, Mar. 2016, Art. no. 023640.
- [23] W. Wang *et al.*, "Anomalous spin-orbit torques in magnetic single-layer films," *Nature Nanotechnol.*, vol. 14, pp. 819–824, Jul. 2019.
- [24] M. Montazeri *et al.*, "Magneto-optical investigation of spin-orbit torques in metallic and insulating magnetic heterostructures," *Nature Commun.*, vol. 6, p. 8958, Dec. 2015.
- [25] H. T. Nembach, J. M. Shaw, C. T. Boone, and T. J. Silva, "Mode- and size-dependent Landau-Lifshitz damping in magnetic nanostructures: Evidence for nonlocal damping," *Phys. Rev. Lett.*, vol. 110, no. 11, Mar. 2013, Art. no. 117201.
- [26] F. Guo, J. M. Bartell, D. H. Ngai, and G. D. Fuchs, "Phase-sensitive imaging of ferromagnetic resonance using ultrafast heat pulses," *Phys. Rev. A, Gen. Phys.*, vol. 4, no. 4, Oct. 2015, Art. no. 044004.
- [27] L. Liensberger, L. Flacke, D. Rogerson, M. Althammer, R. Gross, and M. Weiler, "Spin-wave propagation in metallic Co₂₅Fe₇₅ films determined by microfocused frequency-resolved magneto-optic kerr effect," *IEEE Magn. Lett.*, vol. 10, 2019, Art. no. 5503905.
- [28] T. M. Spicer *et al.*, "Spatial mapping of torques within a spin Hall nanoscillator," *Phys. Rev. B, Condens. Matter*, vol. 98, no. 21, Dec. 2018, Art. no. 214438.
- [29] Z. Q. Qiu and S. D. Bader, "Surface magneto-optic Kerr effect," *Rev. Sci. Instrum.*, vol. 71, no. 3, p. 1243, 2000.
- [30] S. Yoon, J. Liu, and R. D. McMichael, "Phase-resolved ferromagnetic resonance using a heterodyne detection method," *Phys. Rev. B, Condens. Matter*, vol. 93, no. 14, Apr. 2016, Art. no. 144423.
- [31] Y. Li *et al.*, "Optical detection of phase-resolved ferromagnetic resonance in epitaxial FeCo thin films," *IEEE Trans. Magn.*, vol. 55, no. 7, Jul. 2019, Art. no. 6100605.
- [32] Y. Li *et al.*, "Simultaneous optical and electrical spin-torque magnetometry with phase-sensitive detection of spin precession," *Phys. Rev. A, Gen. Phys.*, vol. 11, no. 3, Mar. 2019, Art. no. 034047.
- [33] A. A. Serga, A. V. Chumak, and B. Hillebrands, "YIG magnonics," *J. Phys. D, Appl. Phys.*, vol. 43, no. 26, Jul. 2010, Art. no. 264002.

- [34] *More Information Please See.* [Online]. Available: <https://thatec-innovation.com/>
- [35] Y. Huo, F. L. Zeng, C. Zhou, and Y. Z. Wu, "Spin pumping and thermal effects in single-crystalline Fe/Pt bilayers at the nonresonant condition," *Phys. Rev. A, Gen. Phys.*, vol. 8, no. 1, Jul. 2017, Art. no. 014022.
- [36] S. Klingler *et al.*, "Spin-torque excitation of perpendicular standing spin waves in coupled YIG/Co heterostructures," *Phys. Rev. Lett.*, vol. 120, no. 12, Mar. 2018, Art. no. 127201.
- [37] J. Chen *et al.*, "Strong interlayer magnon-magnon coupling in magnetic metal-insulator hybrid nanostructures," *Phys. Rev. Lett.*, vol. 120, no. 21, May 2018, Art. no. 217202.
- [38] H. Qin, S. J. Hämäläinen, and S. van Dijken, "Exchange-torque-induced excitation of perpendicular standing spin waves in nanometer-thick YIG films," *Sci. Rep.*, vol. 8, no. 1, p. 5755, Dec. 2018.
- [39] Y. Li *et al.*, "Coherent spin pumping in a strongly coupled magnon-magnon hybrid system," *Phys. Rev. Lett.*, vol. 124, Mar. 2020, Art. no. 117202.
- [40] Y. Xiong *et al.*, "Probing magnon-magnon coupling in exchange coupled $Y_3Fe_5O_{12}$ /Permalloy bilayers with magneto-optical effects," *Sci. Rep.*, vol. 10, p. 12548, Jul. 2020.
- [41] G. Gubbiotti, X. Zhou, A. O. Adeyeye, G. Varvaro, and M. Kostylev, "Collective spin waves in arrays of asymmetric and symmetric width nanowires: Effect of the film layering sequence," *J. Phys. D, Appl. Phys.*, vol. 53, no. 13, Mar. 2020, Art. no. 135001.
- [42] J. Chen *et al.*, "Excitation of unidirectional exchange spin waves by a nanoscale magnetic grating," *Phys. Rev. B, Condens. Matter*, vol. 100, no. 10, Sep. 2019, Art. no. 104427.
- [43] E. Albisetti *et al.*, "Optically inspired nanomagnonics with nonreciprocal spin waves in synthetic antiferromagnets," *Adv. Mater.*, vol. 32, no. 9, Mar. 2020, Art. no. 1906439.
- [44] Y. Pogoryelov *et al.*, "Nonreciprocal spin pumping damping in asymmetric magnetic trilayers," *Phys. Rev. B, Condens. Matter*, vol. 101, no. 5, Feb. 2020, Art. no. 054401.